

Transient Hydrodynamic Lattice Cooling by Picosecond Laser Irradiation of Graphite

Jihoon Jeong^{1,*}, Xun Li^{2,*}, Sangyeop Lee^{2,3,†}, Li Shi^{1,4,‡}, and Yaguo Wang^{1,4,§}

¹*Walker Department of Mechanical Engineering, The University of Texas at Austin, Austin, TX 78712, USA*

²*Department of Mechanical Engineering and Materials Science,
University of Pittsburgh, Pittsburgh, PA 15261, USA*

³*Department of Physics and Astronomy, University of Pittsburgh, Pittsburgh, PA 15261, USA*

⁴*Texas Materials Institute, The University of Texas at Austin, Austin, TX 78712, USA*

Recent theories and experiments have suggested hydrodynamic phonon transport features in graphite at unusually high temperatures. Here, we report a pico-second pump-probe thermal reflectance measurement of heat pulse propagation in graphite. The measurement results reveal transient lattice cooling near the adiabatic center of a 15 μm diameter ring-shape pump beam at temperatures between 80 and 120 K. While such lattice cooling has not been reported in recent diffraction measurements of second sound in graphite, the observation here is consistent with both hydrodynamic phonon transport theory and prior heat pulse measurements of second sound in bulk sodium fluoride.

Phonons, the energy quanta of lattice vibration, scatter among themselves via normal (N) and Umklapp (U) processes that conserve and destroy phonon momentum, respectively [1]. The resistivity to heat flow is directly caused by the Umklapp processes and momentum-non-conserving phonon scattering by surface and interior defects. When these resistive processes are dominant, phonon transport is in the diffusive regime described by Fourier's law. When the sample size is smaller than the mean free paths of internal phonon-phonon and phonon-defect scatterings, phonon transport is in the ballistic regime. In comparison to the diffusive and ballistic regimes, phonon hydrodynamics describes a peculiar transport regime that is dominated by N-processes. This regime was predicted by the Peierls-Boltzmann transport theory of phonon gas [2, 3] and experimentally observed at temperatures below 20 K in some bulk crystals [4–8] several decades ago. As stated by Ashcroft and Mermin [9], the observation of the hydrodynamic phonon transport is one of the great triumphs of the theory of lattice vibrations. Hydrodynamic phonon transport received a renewed interest in recent years because of first-principles-based theoretical predictions of phonon hydrodynamics in graphitic materials and other two-dimensional (2D) materials near room temperature, which is relevant to technological applications [10–14].

In the hydrodynamic phonon transport regime, phonon hydrodynamic viscosity [15, 16] associated with frequent N-scattering increases the phonon-boundary scattering mean free paths and thermal conductance of a rod sample compared to the ballistic transport limit [8] due to momentum-conserving random walk of phonons [17]. In addition, upon pulse heating that is faster than the U-processes but slower than the N-processes, a fluctuating temperature field can propagate in the form of a wave with minimal damping. This thermal wave is referred as second sound, analogous to sound wave propagation in a gas as a pressure fluctuation field due to momentum-conserving intermolecular scattering. The second sound

was detected by measuring the temperature evolution at one end of bulk sodium fluoride (NaF) samples at temperatures below 20 K when a heat pulse was applied to the other end [4–7]. Recently, the second sound was observed at temperatures as high as about 100 K in a highly oriented pyrolytic graphite (HOPG) sample using a transient grating experiment that detected the diffraction signal from a thermal expansion grating [18]. Graphite is predicted to exhibit pronounced phonon hydrodynamics due to the presence of a large population of low-frequency flexural modes that undergo frequent momentum-conserving normal scattering [10]. The measurement result is attributed to the appearance of the peak thermal expansion at the middle in between two heated locations, an unusual feature that can only be caused by second sound propagation. However, the diffraction measurement provided relative thermal expansion difference between different locations without differentiating lattice cooling from lattice heating. In addition, this experiment is different from the direct heat pulse measurement [4–7] in the second sound measurements of bulk crystals several decades ago, which revealed detailed thermal fluctuation feature including transient lattice cooling.

In this letter, we report a heat-pulse experiment that is guided by a full solution of the Peierls-Boltzmann transport equation with ab initio inputs to capture the propagation of the second sound in HOPG in space. Below 100 K, we observed a negative displacement of temperature field near the adiabatic center of a 15 μm diameter heating ring formed by a picosecond laser through a pair of axicon lens, that indicated transient cooling of the lattice. The unusual transient lattice cooling observed in this work is a salient feature out of the wave nature of second sound, where the temperature field can fluctuate between positive and negative displacements around the background temperature, similar to the pressure fluctuation of sound propagation in gas. While neither diffusive nor ballistic transport regimes can explain this phe-

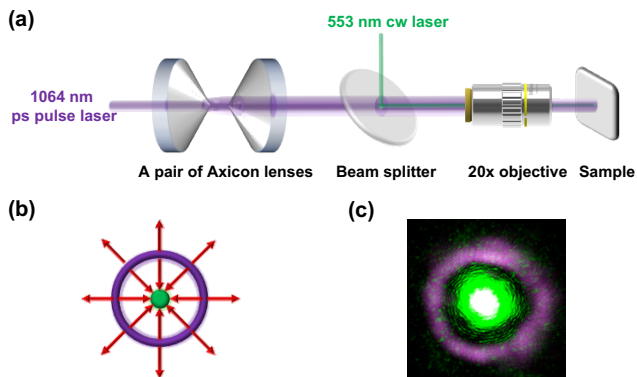


FIG. 1. Experimental setup of optical heat pulse measurement. (a) Schematic diagram of optical heat pulse measurement setup with a pair of axicon lenses to form a ring-shape pump of 1064 nm picosecond pulse laser. Continuous-wave laser at 553 nm wavelength is focused on the center of the ring-shape pump as a probe. (b) Schematic of the ring-shape pump and probe at the center on the sample surface. Red arrows indicate heat propagating directions. (c) An example image of the laser beam on the sample surface.

nomenon, this lattice cooling feature provides a clear evidence and helps advance detailed understanding of the second sound propagation in graphite.

The second sound measurement is implemented with a picosecond transient thermoreflectance (ps-TTR) system [19]. The experiment configuration resembles the heat pulse measurement geometry that was employed for the earliest second sound experiments based on a temperature pulse generator and a bolometer [4, 5, 20], where a temperature pulse generator and a bolometer were directly attached to each side of the millimeter-size bulk samples, and the second sound propagation is in the millisecond time scale.

A noteworthy difference between the experimental setup for NaF several decades ago and for graphite we report here lies in the spatial and temporal scales. The spatial and temporal scales of second sound propagation are closely related to the mean free paths and rates of N- and U-scattering processes. The second sound propagation can have minimal damping when the wavelength of second sound is in between the mean free paths of N- and U-scattering. Similarly, the frequency of second sound should be in between the rates of N- and U-scattering for the clear observation of the second sound [2, 3]. As the second sound in NaF was observed below 20 K where the phonon scattering rates are relatively lower, detection of temperature with millisecond temporal resolution was sufficient. However, the observation of second sound in graphite at much elevated 100 K would require much smaller temporal and spatial resolutions for the experiment. Therefore, the ps-TTR measurement is designed to provide both sub-nanosecond time resolution and micrometer spatial resolutions.

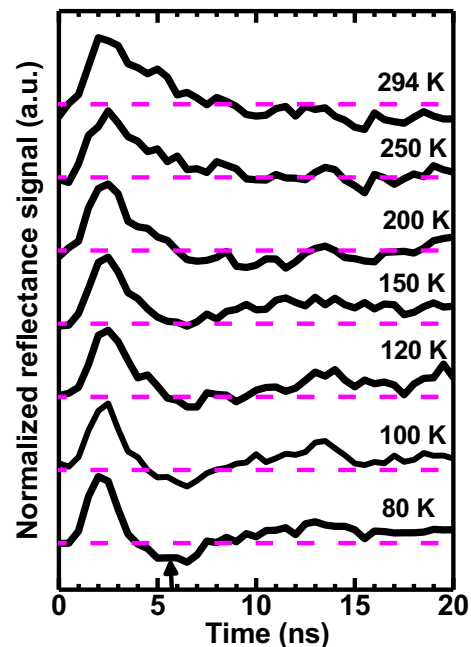


FIG. 2. Normalized reflectance data measured on the LG-HOPG at different temperatures indicated in the figure. The radius of the ring-shape pump is $15 \mu\text{m}$. The arrow indicates lattice cooling due to second sound propagation. (Note: all the reflectance signals plotted in Fig. 2, Fig. 3 and Fig. 4 are negative values. This is a more convenient way to illustrate the lattice cooling effect because the dR/dT coefficient is negative for graphite.)

Our measurement uses a picosecond laser of 1064 nm wavelength (1 mW) as the pump to deliver a heating pulse of 400 ps at 10 kHz repetition rate to the HOPG sample, which is attached with a silver paste to the sample stage of a continuous flow cryostat. A continuous-wave (cw) laser of 553 nm wavelength (1 mW) is employed as a probe, the reflectance of which is detected by the avalanche photodiode (APD) with 500 ps resolution. Even though the 400 ps pump pulse can excite hot electrons that would scatter with phonons and induce nonequilibrium phonon populations, the effects of electron-phonon coupling (on a time scale of less than 10 ps) [21] and phonon-phonon thermalization (on a time scale of less than 500 ps) [13] are not considered here, because they both occur on time scales shorter than that of the phenomenon observed here (500 ps \sim 20 ns). In addition, hot electron diffusion length is less than $2 \mu\text{m}$ in thick graphene [21], much shorter than the separation distance between the pump and probe ($>10 \mu\text{m}$). Therefore, it is reasonable to attribute the observed phenomena to lattice cooling/heating only. A pair of axicon lenses is used to form a ring-shape pump beam focused on the sample surface through another 20x objective lens, as shown in Fig. 1(a). The probe beam is delivered to the center of the pump beam on the sample surface to

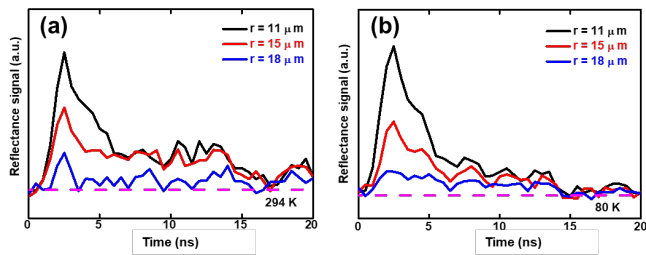


FIG. 3. Normalized reflectance data measured on the SG-HOPG at (a) 294 K and (b) 80 K. The measurement was conducted at three different radii (r) of the ring-shape pump, including 11, 15, 18 μm . The horizontal dashed line indicates zero temperature rise.

detect the heat pulse propagation, as shown in Fig. 1(b). The $1/e^2$ diameter of the Gaussian probe beam size is 6 μm , and the pump ring width is 3 μm . The average radius of the ring-shape pump beam is calculated as the mean value of inner and outer radii of the ring and is used to estimate the average distance between the pump and probe and the heat pulse propagation distance. Since the in-plane thermal conductivity of graphite is up to 300 times higher than the cross-plane thermal conductivity, the probe beam detects mainly the heat propagation along the basal plane.

The same heat pulse measurements are conducted on two different commercial HOPG samples with different grain sizes, 10 \sim 20 μm for a SPI grade-1 sample denoted as LG-HOPG and shown in Fig. S1 and 30 \sim 40 nm for a SPI grade-3 sample referred here as SG-HOPG. Fig. 2 shows the probe signal measured at the center of the 15 μm diameter ring-shape pump beam on the LG-HOPG sample at temperature between 300 K and 80 K. Above 150 K, the thermoreflectance signal first arises to the peak and then relaxes to its initial value. This behavior exhibits an ordinary thermal decay that is expected for diffusive phonon transport. As the temperature decreases down to below 120 K, a narrow positive peak appears at about 2 ns delay time, which is followed by a negative peak at around 6 ns. The negative peak becomes increasingly clear when the sample stage temperature decreases further to 80 K. In comparison, the negative temperature displacement is not observed in the SG-HOPG sample at temperatures between 294 and 80 K, as shown in Fig. 3. For three different radii of the ring-shape pump beam, the thermoreflectance signal consistently shows lattice temperature increases and then decays in time in this small-grain size graphite sample.

When the probe beam is moved to a position about 8.8 μm away from the adiabatic center of the ring-shape pump beam, the negative temperature rise can still be observed, as shown in Fig. S2. However, when the probe beam is moved to overlap with the ring-shape pump, the

temperature rise becomes always positive [22]. We also tested a case without axicon lens, where a Gaussian pump beam and a Gaussian probe beam are offset from each other, the observed temperature rise at the probe beam location is also always positive, as shown in Figs. S3 and S4 [22]. The negative temperature displacement, which indicates lattice cooling, cannot occur in either the diffusive or the ballistic transport regime. In the diffusive regime, the pump beam results in a temperature rise that propagates in space and decays monotonically in time. In the ballistic regime, different phonon polarizations give rise to the propagation of discrete heat pulses that only increases the lattice temperature. In comparison, in the purely hydrodynamic regime where the total momentum of phonons is conserved, the temperature field can fluctuate between positive and negative displacements without any damping, similar to the pressure fluctuation during sound propagation in gas. The presence of U-scattering results in damping of the fluctuation of the temperature field. Such a damped fluctuation is only observed in the thermoreflectance signal of the large-grain size HOPG sample. Despite the damping, the negative temperature displacement provides an unambiguous evidence of phonon hydrodynamics caused by dominant N-scattering processes in graphite at temperatures between 80 and 120 K.

To better understand the lattice cooling feature that is observed only near the center of the ring-shape pump beam, we simulated the heat-pulse experiment by solving the Peierls-Boltzmann transport equation in time, real space, and reciprocal space domains with ab initio inputs. To account for the strong N-scattering, the simulation is based on a full matrix of three-phonon scattering instead of commonly used single mode relaxation time approximation [15, 23]. The simulation considers the same Gaussian probe beam at the center of the ring-shape heating pulse as in the experiment (Fig. S6). The dimension of the simulated HOPG sample is 20 $\mu\text{m} \times 20 \mu\text{m} \times 1 \mu\text{m}$ [22]. The simulation results in Fig. 4 reveal the evolution of temperature profile during the heat-pulse experiment. As shown in Fig. 4(a-b), the applied ring-shape heat pulse propagates toward the center within 2.1 ns following the pulse heating. At 3.5 ns, the heat pulse travelling from the ring-shape heater merges at the center in Fig. 4(c). Subsequently, the heat pulse propagates outward in Fig. 4(d), resulting in negative temperature rise near the center as shown in Fig. 4(e). The evolution of the temperature profile is summarized in Fig. 4(f) to show the clear fluctuation of temperature field at the adiabatic center upon the arrival and departure of the heat pulse. The negative peak predicted is in qualitative agreement with the experimental observations, as shown in Fig. 4(g). The interval between the first peak and the cooling center is around 4 \sim 4.5 ns, and a drift speed of second sound can be estimated as 3333 \sim 3750 m/s, consistent with the second sound speed [18]. This estimated

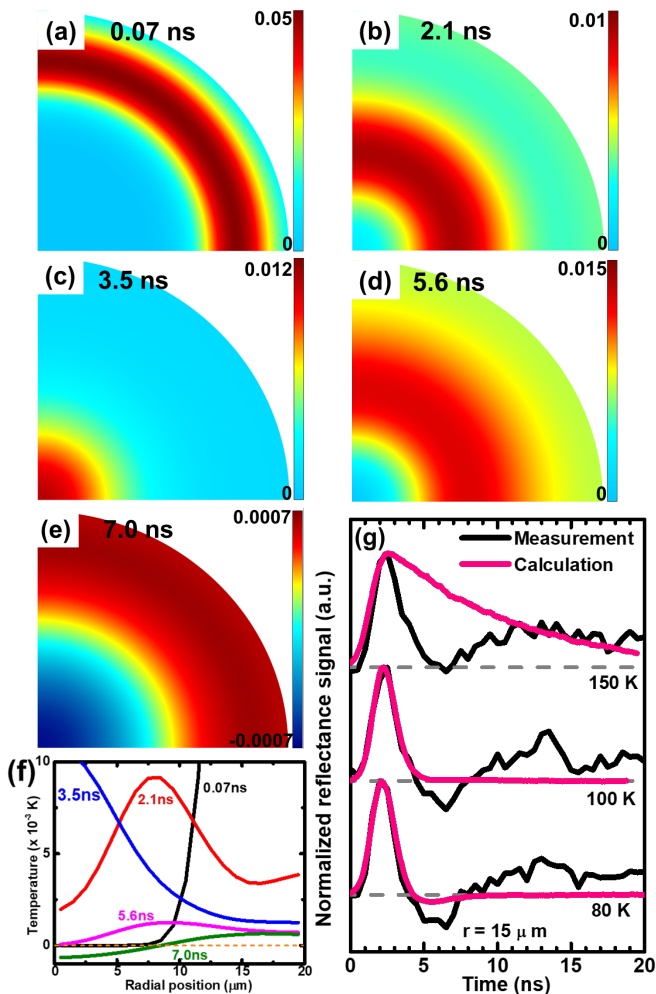


FIG. 4. (a-e) Snapshots of the calculated transient temperature profiles on the top surface of a graphite sample irradiated by a $15 \mu\text{m}$ radius pump beam at an ambient temperature of 80 K. The heat pulse propagates inward in (a-c), then outward in (d), leaving negative temperature rise at the adiabatic center in (e) due to the hydrodynamic thermal fluctuation. (f) Evolution of the temperature profile along the radial direction at each time. (g) Comparison between the experiment and the calculation results for a pump beam radius of $15 \mu\text{m}$ at three different temperatures of 80, 100, and 150 K.

speed is different from the speed of sound in graphite, which is $12.3 \sim 14.7 \text{ km/s}$ for LA phonon mode and $21 \sim 22.2 \text{ km/s}$ for TA phonon mode. These “first” sound waves generated at pump position would reach the probe position (center) between 0.7 ns and 1.2 ns, much faster than the second sound observed here [24, 25].

The negative temperature rise observed at the center resembles the results of heat-pulse experiments performed with a bulk NaF sample [5]. In the previous report, the temporal temperature profile recorded by a bolometer at the adiabatic end of the bulk sample shows the negative temperature rise upon the arrival of the sec-

ond sound peak. In our experimental setup with a ring-shape pump, the probe is at the center that is a thermally adiabatic boundary due to the central symmetry. In both the past experiment in NaF [5] and our experiment, the negative temperature rise occurred after the second sound pulse is reflected by a thermally adiabatic boundary.

The adiabatic boundary appears to be an important condition for observing the lattice cooling. Indeed, no lattice cooling is observed in both simulation and experiment when the Gaussian pump beam is offset from a Gaussian probe beam [22]. Thus, our experimental setup with the ring-shape pump and probe at the center provides a unique approach to achieve the adiabatic boundary condition at the center probe location, this ring-shape heating configuration also avoids the local strain that can be generated by the tightly focused pump and probe beams that overlap with each other. In comparison, an adiabatic boundary condition is also achieved at the middle point between two heating lines in the recently reported diffraction grating measurement of second sounds of graphite [18]. However, the diffraction measurement does not measure the local temperature rise exactly at that middle point. Instead, the diffraction signal is influenced by the spatial distribution of the thermal expansion signal over the entire large probe region without revealing whether lattice cooling could occur at the thermally adiabatic boundary or not.

It is not possible to observe such a temperature fluctuation in the diffusive or ballistic regime. In the diffusive regime, phonons do not propagate as a collective motion. The temperature rise excited by the pump beam decays monotonically in time. The solutions of the energy conservation equation with the Fourier’s law always produce an exponential decay of temperature in time and space and cannot yield temperature field that fluctuates between positive and negative displacements. The excess phonon momentum gained from laser heating is destroyed locally in space by strong Umklapp scattering, and non-local effect is not possible. In addition, there is no mechanism that can lead to the cooling effect while phonons are relaxed to local equilibrium from a temperature rise. In the ballistic regime, there is no damping of the energy when phonons propagate from pump position to probe position. The lattice temperature would only increase.

In Fig. 4(f), the negative dips predicted with simulation are much shallower than those measured, indicating a weaker phonon hydrodynamic effect produced in calculations. Our current simulations only account for the lowest-order anharmonicity that induces three-phonon scattering. High-order anharmonicity and the associated four-phonon scattering processes are not considered. A recent calculation with empirical potential has suggested that four-phonon scattering is also impor-

tant in graphene [26]. Normal scattering among four small-wavevector phonons can potentially lead to more pronounced transient hydrodynamic lattice cooling effect than the existing calculation result. Neglecting the four-phonon scattering process in our current calculations may be the reason of weaker hydrodynamic effect predicted than experiments.

In summary, our measurement results reveal that, due to hydrodynamic phonon transport, the pulse heating can create lattice cooling near the adiabatic boundary several micrometers away from the heat source in graphite at temperatures between 80 and 120 K. This feature is consistent with both theoretical calculation for graphite and prior second sound measurements of bulk NaF, but cannot be unambiguously revealed from the recent diffraction measurement of second sound in graphite. Therefore, the experimental observation reported here provides detailed insight into the hydrodynamic transport behaviors in graphite.

This work is supported by two collaborative awards (CBET-1705756 and CBET-1707080) from the National Science Foundation. The simulation was performed using the Linux cluster of the Center for Research Computing at the University of Pittsburgh.

* These authors contributed equally to this work

† sylee@pitt.edu

‡ lishi@mail.utexas.edu

§ yaguo.wang@austin.utexas.edu

- [1] R. Peierls, *Annalen der Physik* **395**, 1055 (1929).
- [2] R. Guyer and J. Krumhansl, *Physical Review* **148**, 778 (1966).
- [3] R. A. Guyer and J. Krumhansl, *Physical Review* **148**, 766 (1966).
- [4] C. Ackerman and W. Overton Jr, *Physical Review Letters* **22**, 764 (1969).
- [5] H. E. Jackson, C. T. Walker, and T. F. McNelly, *Physical Review Letters* **25**, 26 (1970).
- [6] T. McNelly, S. Rogers, D. Channin, R. Rollefson, W. Goubau, G. Schmidt, J. Krumhansl, and R. Pohl, *Physical Review Letters* **24**, 100 (1970).
- [7] V. Narayanamurti and R. Dynes, *Physical Review Letters* **28**, 1461 (1972).
- [8] L. Mezhev-Deglin, *Sov. Phys. JETP* **22**, 47 (1966).
- [9] N. W. Ashcroft and N. D. Mermin, Saunders College, Philadelphia (1976).
- [10] S. Lee, D. Broido, K. Esfarjani, and G. Chen, *Nature communications* **6**, 6290 (2015).
- [11] A. Cepellotti, G. Fugallo, L. Paulatto, M. Lazzeri, F. Mauri, and N. Marzari, *Nature communications* **6**, 6400 (2015).
- [12] S. Lee and L. Lindsay, *Physical Review B* **95**, 184304 (2017).
- [13] Z. Ding, J. Zhou, B. Song, V. Chiloyan, M. Li, T.-H. Liu, and G. Chen, *Nano letters* **18**, 638 (2018).
- [14] L. Shi, *Science* **364**, 332 (2019).
- [15] X. Li and S. Lee, *Physical Review B* **97**, 094309 (2018).
- [16] C. Ackerman and R. Guyer, *Annals of Physics* **50**, 128 (1968).
- [17] R. Gurzhi, *Sov. Phys. JETP* **19**, 490 (1964).
- [18] S. Huberman, R. A. Duncan, K. Chen, B. Song, V. Chiloyan, Z. Ding, A. A. Maznev, G. Chen, and K. A. Nelson, *Science* **364**, 375 (2019).
- [19] J. Jeong, X. Meng, A. K. Rockwell, S. R. Bank, W.-P. Hsieh, J.-F. Lin, and Y. Wang, *Nanoscale and Microscale Thermophysical Engineering* **23**, 211 (2019).
- [20] T. F. McNelly, PhDT (1974).
- [21] K. Chen, M. N. Yogeesh, Y. Huang, S. Zhang, F. He, X. Meng, S. Fang, N. Sheehan, T. H. Tao, S. R. Bank, *et al.*, *Carbon* **107**, 233 (2016).
- [22] See Supplemental Material.
- [23] C. D. Landon and N. G. Hadjiconstantinou, *Journal of Applied Physics* **116**, 163502 (2014).
- [24] A. Bosak, M. Krisch, M. Mohr, J. Maultzsch, and C. Thomsen, *Physical Review B* **75**, 153408 (2007).
- [25] X. Cong, Q.-Q. Li, X. Zhang, M.-L. Lin, J.-B. Wu, X.-L. Liu, P. Venezuela, and P.-H. Tan, *Carbon* **149**, 19 (2019).
- [26] T. Feng and X. Ruan, *Physical Review B* **97**, 045202 (2018).

Supplemental Material: Transient Hydrodynamic Lattice Cooling by Picosecond Laser Irradiation of Graphite

Jihoon Jeong^{1,*}, Xun Li^{2,*}, Sangyeop Lee^{2,3,†}, Li Shi^{1,4,‡} and Yaguo Wang^{1,4§}

¹Walker Department of Mechanical Engineering, The University of Texas at Austin, Austin, TX 78712, USA

²Department of Mechanical Engineering and Materials Science,
University of Pittsburgh, Pittsburgh, PA 15261, USA

³Department of Physics and Astronomy, University of Pittsburgh, Pittsburgh, PA 15261, USA

⁴Texas Materials Institute, The University of Texas at Austin, Austin, TX 78712, USA

(Dated: May 24, 2021)

1. Grain size measurement of the large-grain size HOPG sample

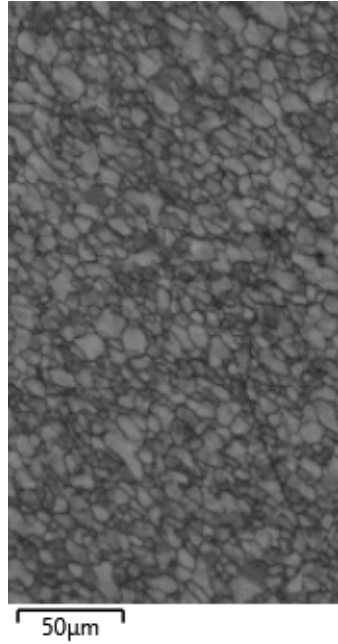


FIG. S1. Electron backscatter diffraction (EBSD) image of the top-surface of the large-grain size HOPG sample.

2. Off-center probe measurement results with a ring-shaped pump beam

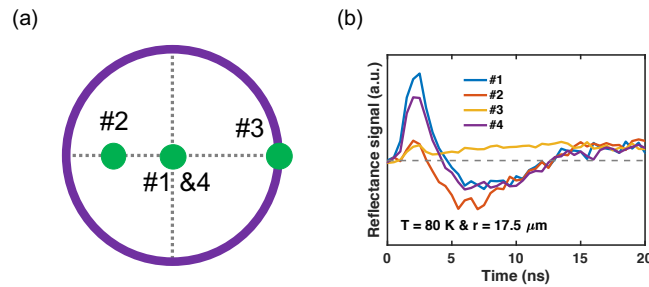


FIG. S2. (a) Schematic illustration of the off-center probe measurement configuration. The purple ring is the 17.5- μm -radius pump beam. The green circle represents the probe location of four different measurements. (b) Reflectance signal obtained from each of the four probe locations indicated in (a).

3. Regular pump-probe measurement results on graphite

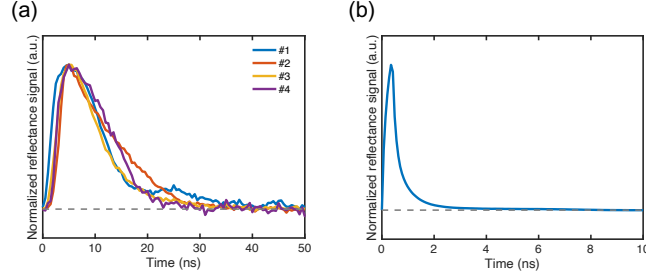


FIG. S3. (a) Normalized reflectance signal from a regular pump-probe measurement where the $6\text{-}\mu\text{m}$ -radius Gaussian pump and the $6\text{-}\mu\text{m}$ -radius Gaussian probe beams are at the same location. (b) Monte Carlo simulation results of the regular pump-probe measurement

4. Offset pump-probe measurement

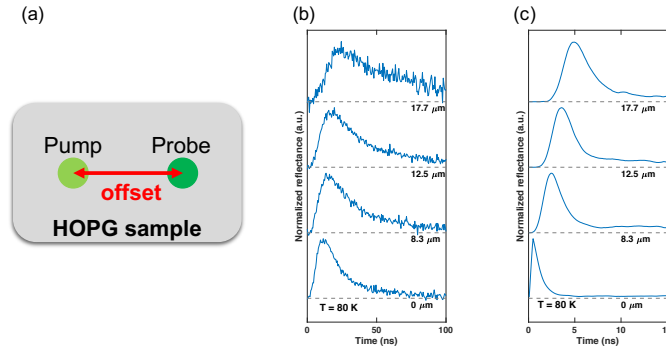


FIG. S4. (a) Schematic diagram of the offset pump-probe measurement. (b) Experimental and (c) simulation results of the offset pump-probe measurement with the different pump-probe offset distance of 0, 8.3, 12.5, and $17.7\text{ }\mu\text{m}$.

5. Thermoreflectance coefficient of graphite

The thermoreflectance coefficient (dR/dT) of graphite is smaller than those of metal transducers but sensitive enough for detecting thermal decay. As shown in Fig. S5(a), we measured the photodiode signal (mV), considered as the reflectance, at different pump power for our HOPG sample at 532 nm wavelength using a reported method [1]. The measured photodiode signal change versus temperature change is about -4.8 mV/K , which can be used to convert the measured peak reflection signal to a temperature rise of 0.52 K (e.g. $[-2.5\text{ mV}] / [-4.8\text{ mV/K}]$). The powers of pump and probe lasers are both 1 mW. Within this power range, the yielded temperature modulation is small enough that the response is linear. Fig. S5(b) shows the raw experimental data before normalization.

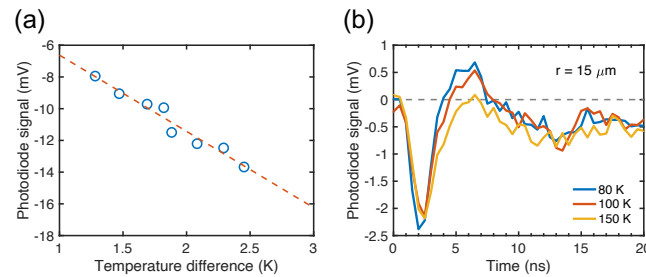


FIG. S5. (a) The photodiode signal versus temperature change measurement data for graphite at 532 nm wavelength and (b) the raw experimental data with amplitude indicated. Since the photodiode signal versus temperature change is negative, the raw data plot shows a negative peak for a positive temperature change.

6. The ring-shape pump

Fig. S6 shows an example image of a ring-shape pump and the intensity contour plot converted from the example image using MATLAB. The intensity of the pump pulse in the center of the ring is negligible compared to the ring region. Within the ring region, the intensity profile has a Gaussian shape. Since the probe position is in the center of the ring, the probed signal comes from the propagating heat pulse generated at the ring region. As shown in the supplemental Material (part 2), we scanned different probe locations to see whether the signal deforms to any other shape. The overall traces keep the same unless the probe overlaps with the pump ring.

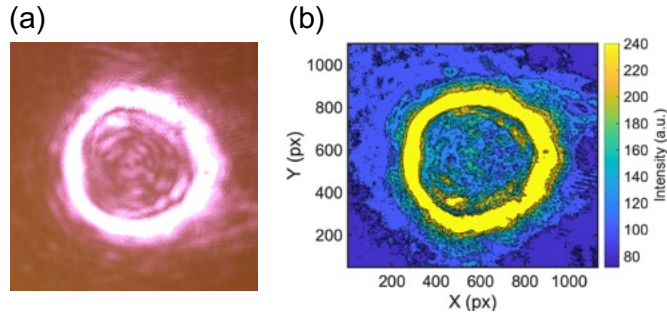


FIG. S6. (a) An example image of a ring-shape pump with a diameter of 21 μm and a thickness of 3 μm and (b) the intensity contour plot using MATLAB with a contour intensity scale of 0-255 (right). The blue region reflects the intensity of background, including white light in the imaging system.

7. Schematic of a 3D graphite sample of the Monte Carlo simulation

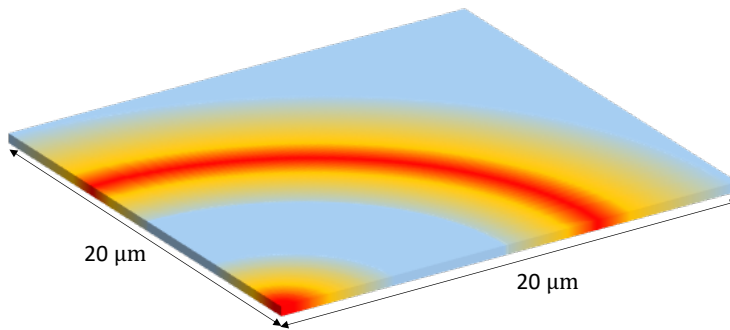


FIG. S7. Schematic of a 3D graphite sample for the Monte Carlo simulation. One quarter of the experimental setup is simulated, with adiabatic boundaries for the front, left, and top surfaces. The back, right, and bottom surfaces are at constant ambient temperature. The sample thickness is 1 μm .

8. Details of the Monte Carlo simulation

The propagation of second sound in bulk graphite can be simulated by solving the Peierls-Boltzmann equation (PBE). The transient PBE with a full scattering matrix is

$$\frac{\partial f_i(\mathbf{r}, t)}{\partial t} + \mathbf{v}_i \cdot \nabla_{\mathbf{r}} f_i(\mathbf{r}, t) = \sum_j C_{ij} f_j(\mathbf{r}, t) \quad (\text{S1})$$

where i indicates a phonon state, f is the phonon distribution function, \mathbf{v} is the phonon group velocity, \mathbf{r} is the position vector in the three-dimensional real space, t is time, and C_{ij} is the element of scattering matrix \mathbf{C} . The transient PBE was solved by a deviational Monte Carlo (MC) method [2, 3] with inputs of phonon dispersion and scattering matrix from first-principles calculations.

The first-principles calculations were performed using the Vienna Ab initio Simulation Package [4-6]. We used the projector-augmented-wave pseudopotentials and local density approximation for exchange-correlation energy functional. The van der Waals interaction was included with a non-local correlation functional, optB88-vdW [7, 8]. The cutoff energy of the plane wave basis is 520 eV. The crystal structure was relaxed with a $24 \times 24 \times 10$ grid for sampling electronic states (k points) in the first Brillouin zone. The second order force constants were calculated by density

functional perturbation theory with $5 \times 5 \times 2$ supercells. The third order force constants were calculated by a real space supercell approach with $4 \times 4 \times 2$ supercells and $8 \times 8 \times 6$ grid of k points, with a cut-off distance to the fifth nearest neighbor. The phonopy [9] and thirdorder.py [10] packages were also used in the calculations of second and third order force constants, respectively.

The deviational MC method has been used to study steady-state thermal transport in two-dimensional graphene ribbons [2, 3, 11, 12], and the details of the algorithm can be found in these literatures. Here we implemented the MC method for transient phonon transport with a heating source in three-dimensional crystalline graphite. The sample geometry and the boundary conditions are shown in Fig. S5. The sample thickness was chosen to be $1 \mu\text{m}$, which is much larger than the thermal penetration depth of 200 nm estimated from the heat diffusion equation. For the front, left, and top surfaces of the sample, thermally adiabatic boundary condition was applied. The adiabatic surfaces reflect incoming phonons specularly, so only one quarter of the experimental setup is needed because of the symmetry in the in-plane transport. For the entire sample, the phonon distribution was initialized with the equilibrium Bose-Einstein distribution at a homogenous ambient temperature. The sample was discretized into $20 \times 20 \times 3$ control volumes in the real-space domain. The first Brillouin zone of reciprocal space was discretized with a $25 \times 25 \times 5$ grid. The time space was discretized with a time interval of 7, 5, and 3 ps at 80, 100, and 150 K, respectively. The heating by the pump laser which has a ring-shape was simulated by applying heat source to the control volumes for the time duration of actual laser (400 ps). The intensity of heat source follows the Gaussian distribution with the same full width at half maximum (FWHM) value as the pump beam used in the experiment ($3 \mu\text{m}$) along the in-plane direction. In the process of heating, phonons were generated following the equilibrium Bose-Einstein distribution at local temperature. The time-and-space-dependent phonon distribution function was calculated to sample the local temperature change. The temporal temperature change at the dot-shape probe beam was collected by averaging the local temperatures weighted by a Gaussian function with a FWHM of $3 \mu\text{m}$, which is the same as the actual probe beam used in the experiment.

* These authors contributed equally to this work

† sylee@pitt.edu

‡ lishi@mail.utexas.edu

§ yaguo.wang@austin.utexas.edu

- [1] R. Wilson, B. A. Apgar, L. W. Martin, and D. G. Cahill, *Optics express* **20**, 28829 (2012).
- [2] C. D. Landon and N. G. Hadjiconstantinou, *Journal of Applied Physics* **116**, 163502 (2014).
- [3] X. Li and S. Lee, *Physical Review B* **97**, 094309 (2018).
- [4] G. Kresse and J. Furthmüller, *Computational Materials Science* **6**, 15 (1996).
- [5] G. Kresse and J. Furthmüller, *Phys. Rev. B* **54**, 11169 (1996).
- [6] G. Kresse and D. Joubert, *Physical Review B* **59**, 1758 (1999).
- [7] J. Klimeš, D. R. Bowler, and A. Michaelides, *Journal of Physics: Condensed Matter* **22**, 022201 (2009).
- [8] J. Klimeš, D. R. Bowler, and A. Michaelides, *Physical Review B* **83**, 195131 (2011).
- [9] A. Togo and I. Tanaka, *Scripta Materialia* **108**, 1 (2015).
- [10] W. Li, J. Carrete, N. A. Katcho, and N. Mingo, *Computer Physics Communications* **185**, 1747 (2014).
- [11] X. Li and S. Lee, *Physical Review B* **99**, 085202 (2019).
- [12] S. Lee, X. Li, and R. Guo, *Nanoscale and Microscale Thermophysical Engineering* **23**, 247 (2019).